RSC Advances

PAPER

View Article Online
View Journal | View Issue

Cite this: *RSC Adv.*, 2017, **7**, 49777

CO_2-switchable polymer-hybrid silver nanoparticles and their gas-tunable catalytic activity†

Zanru Guo,[a] Hongjian Gu,[a] Wei Ma,[a] Qiang Chen,[a] Zhanfeng He,*[b] Jiali Zhang,[a] Yongxin Liu,[a] Longzhen Zheng[a] and Yujun Feng *[c]

Received 21st August 2017
Accepted 9th October 2017

DOI: 10.1039/c7ra09233d

rsc.li/rsc-advances

The design of controllable or "signal-triggered" metal nanoparticles is one of the emerging trends in nanotechnology and advanced materials. CO_2-switchable polymer-hybrid silver nanoparticles (AgNPs) were prepared by a one-pot reaction reducing $AgNO_3$ and trithioester terminated PDEAEMA with sodium borohydride ($NaBH_4$). The hybrids showed a long-term stability, and their size and size distribution can be easily modulated by tuning the molar ratio of polymers to $AgNO_3$. The hybrids not only exhibit hydrophobic–hydrophilic transitions in immiscible mixed solvents, but also undergo a switchable dispersion/aggregation states upon alternately treating with CO_2 and N_2. Moreover, this smart hybrid was preliminarily used as catalyst for the reduction of 4-nitrophenol. The catalytic activity of the hybrids can be switched and monotonously tuned by varying the flow rate of CO_2 purged into the reaction system, which may open a new avenue for tailoring the catalytic activity of metal nanoparticles toward a given reaction.

Introduction

In recent years, metal nanoparticles (NPs) such as Au and Ag, have garnered much interest, especially in the field of catalysts, owing to their unusual physicochemical properties that are quite different from those of the bulk solids or atomic state.[1–5] However, metal NPs are biased toward self-aggregation to form big particles due to their high surface energy,[6] which not only severely hinders their long-term storage and processing but also reduces their catalytic activity.[7–9] To counter this problem, several supported agents such as surfactants,[10] solid surface,[11] polyelectrolyte brushes,[12] hollow capsules,[13] dendrimers[14] and hydrogels[15] have been exploited to make metal NPs dispersed or individualized. Recently, metal NPs were studied for application in "smart" catalysts with switchable, tunable and reusable catalytic properties.[9,16–23] To be successfully applied, metal NPs should be not only dispersed but also sensitive to external stimulus.[9,16–23] Functionalization of metal NPs with stimuli-responsive polymers represents one of the choices to satisfy such requirements.

Up to date, several kinds of stimuli-responsive polymers have been used to functionalize metal NPs to form "smart" catalysts. For example, temperature-responsive polymeric hydrogel,[24] micelle,[25,26] microgel,[27] "yolk–shell" structure,[28] and polymers[29] were employed to support metal NPs, forming temperature switchable or tunable catalysts. Similarly, metal NPs were immobilized in pH-responsive polymeric hydrogel,[30,31] microsphere,[32] and micelle[33] to get pH-responsive catalytic systems. Besides, light-controllable catalyst was obtained by the combination of a temperature-responsive polymer with metal nanoparticles which can convert light into heat through light irradiation.[9] Though the use of temperature as a trigger for metal "smart" catalysts can switch reaction and modulate reaction rate, changing reaction temperature would result in some side reaction or affect reaction rate,[9] which lead to a nonmonotone correlation with temperature. As for pH trigger based on acids and bases, it is hard to tune reaction rate as reaction usually happened in a fix pH range.[23,31] Moreover, the use of acids and bases for tuning pH may contaminate or modify the final products.[9] Therefore, to switch catalytic activity and modulate catalytic rate, it is desirable to develop a "green" and simple trigger for metal "smart" catalysts.

Very recently, we and others have employed CO_2 and inert gas such as nitrogen to switch between the hydrophobic and hydrophilic property of polymers with amidine[34,35] or amino groups,[36–40] and then control the morphology of

[a]*Department of Polymer Materials and Chemical Engineering, School of Materials Science and Engineering, East China Jiaotong University, Nanchang, Jiangxi 330013, P. R. China. E-mail: guozanru@ecjtu.edu.cn*

[b]*State Key Laboratory of Oil and Gas Reservoir Geology, Exploitation Southwest Petroleum University, Chengdu 610500, P. R. China. E-mail: he_zhanfeng2008@126.com*

[c]*Polymer Research Institute, State Key Laboratory of Polymer Materials Engineering, Sichuan University, Chengdu 610065, P. R. China. E-mail: yjfeng@scu.edu.cn*

† Electronic supplementary information (ESI) available: ^{1}H NMR and GPC of polymers, IR spectra, XRD data and TEM images of hybrids, the data of catalysis and pH variation during the catalytic process and some calculations. See DOI: 10.1039/c7ra09233d

nanomaterials[34,40] or its self-assemblies.[36,39] As an abundant, economical, nontoxic, biocompatible, and renewable resource, CO_2 trigger just bubble gas and leave no contamination during the stimulate process,[34–39] which may satisfy the requirements of metal "smart" catalysts. Zhao and coworkers[41] pioneered the fabrication of CO_2-switchable gold nanoparticles (AuNPs) by functionalizing AuNPs with CO_2-switchable polymers, and found the obtained AuNPs hybrids can be dispersed–re-dispersed in and separated from aqueous solution by CO_2 and N_2 bubbling. Besides, the hybrids exhibit high catalytic activity, easier separation and better reusability for 4-nitrophenol reduction. Yuan *et al.*[42] embedded AuNPs into the shell of CO_2-responsive magnetic hybrid nanospheres, and switch their catalytic activity through the access of swollen or collapsed of CO_2 sensitive shell. Although these metal hybrid catalysts exhibit CO_2-responsive properties, the studies were focused on gold metal, and its reusability and switchability. To the best of our knowledge, there have been few reports of other CO_2-responsive metal catalyst and the gas-modulated catalytic activity. Compared with AuNPs and other metal nanoparticles (like Pt, Pd),[43,44] silver nanoparticles (AgNPs) can be prepared more readily and inexpensively and also exhibits similar catalytic properties, which may have broad application prospects in catalysis.[45] As such, the appeal for CO_2-switchable AgNPs with gas-tunable catalytic activity for the general development of smart catalysts remains high.

In this report, we used an reversible addition–fragmentation transfer polymerization (RAFT) technique to synthesize a CO_2-responsive polymer poly(2-(diethylamino)-ethyl methacrylate) (PDEAEMA), since RAFT polymerization has the advantage to prepare the thiol terminated polymer because the chain transfer agents always contain the dithioester or trithioester group that can be easily reduced to thiol terminated group.[46–48] Resorting to reducing agent sodium borohydride ($NaBH_4$), $AgNO_3$ and trithioester end group of PDEAEMA were reduced to silver nanoparticles (AgNPs) and thiol moiety, respectively; then PDEAEMA adsorbed onto the surface of AgNPs *via* strong Ag–sulfur interaction, forming PDEAEMA–AgNPs (Ag–P) hybrids (Scheme 1). The hydrophilic–hydrophobic properties and dispersibility of the AgNPs were examined by bubbling CO_2 or N_2. The hybrids were applied as a catalyst in a model catalytic reduction of 4-nitrophenol, as it is one of the most refractory pollutants that can occur in industrial waste waters.[42,48] Besides, the catalytic activity at different CO_2 flow rate was preliminarily discerned, which may open a new avenue for tailoring the catalytic activity of metal nanoparticles toward a given reaction.

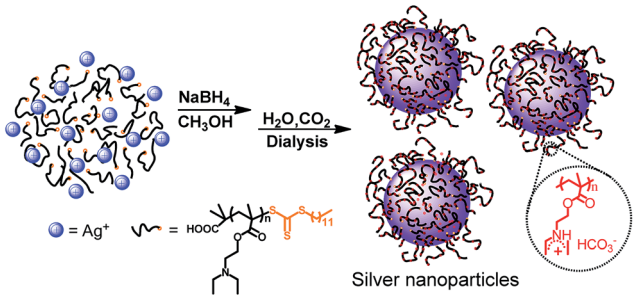

Scheme 1 Schematic representation of the formation of polymer-hybrid silver nanoparticles.

Experimental

Materials

2-Diethylaminoethyl methacrylate (DEAEMA, ≥99.5%), silver nitrate ($AgNO_3$, ≥99.8%), and sodium borohydride ($NaBH_4$, ≥98%) were purchased from Aladdin co., Ltd. 2,2′-Azoisobutyronitrile (AIBN) (Aldrich, 98%) was recrystallized from diethylether prior to use. The chain transfer agent (CTA), *S*-1-dodecyl-*S*′-(α,α′-dimethyl-α″-aceticacid)trithiocarbonate, was synthesized following a previously reported procedure.[49] All the chemicals were used as received, and all aqueous solutions were prepared with deionized water.

Preparation of PDEAEMA

PDEAEMA with trithioester terminal group was prepared *via* RAFT polymerization. DEAEMA (6.0 g, 0.032 mol), AIBN (21 mg, 0.128 mmol), and CTA (0.23 g, 0.64 mmol) were added into a three-necked flask, followed by the addition of 30 mL of THF. After bubbling with nitrogen for at least 30 min, the reaction was heated to 70 °C for 24 h. Then the polymerization was quenched by immerging the reaction flask into liquid nitrogen for about 5 minutes. The product mixture was diluted by 10 mL THF, and the final product was gained *via* precipitation in cold *n*-hexane (−78 °C, *ca.* 500 mL) followed by filtration over a G4 frit. The obtained product was redissolved in 20 mL THF and reprecipitated in cold *n*-hexane (−78 °C, *ca.* 500 mL) again. The resultant solid was collected by filtration and dried overnight in a vacuum oven for 24 h to give PDEAEMA. Yield: 5.45 g (~85%).

Preparation of silver nanoparticles

Different molar ratios (1 : 24, 1 : 12 and 1 : 6) of PDEAEMA to $AgNO_3$ were investigated, and PDEAEMA-stabilized silver nanoparticles (Ag–P) dispersions were prepared by the reduction of $AgNO_3$ using $NaBH_4$ in methanol solution. The ratio of polymer to silver (1 : 24) is as an example: 0.192 g of PDEAEMA was dissolved in 50 mL of methanol. 0.081 g of $AgNO_3$ was dissolved in 2 mL of deionized water, and the solution of $AgNO_3$ was added into the PDEAEMA solution drop by drop under vigorous stirring (1200 rpm). After stirring for 30 minutes, 0.359 g of $NaBH_4$ solid was slowly added to the mixed solution with stirring. The appearance of the mixture immediately changed from light yellow to dark brown. After stirring for 24 h, the mixture was concentrated to *ca.* 10 mL by rotary evaporator. Then 2 mL of water was added with bubbling CO_2 (30 mL min^{-1}), which does not have solid precipitation. After bubbling for 30 minutes, another 2 mL of water was added. The above procedure was repeated until 10 mL of deionized water was added. Then the mixture was dialyzed against distilled water for one week to remove methanol, sodium borate and other unreacted impurities. The distilled water was changed every 4 h during the dialysing. Finally, the polymer-hybrid silver nanoparticles dispersion was obtained.

Catalytic reduction of 4-nitrophenol

Referring to previous methods,[55] 1 mL of 2.5 mM 4-nitrophenol and 1 mL of 250 mM $NaBH_4$ solution was diluted by 23 mL of distilled water in a 50 mL beaker, the mixture was stirred for 5 min at room temperature. Then, the mixture was transferred to a test tube and 0.01 mL of 5 mg mL^{-1} silver nanoparticle dispersion was added, the mixture was taken out for UV-vis adsorption monitoring immediately. Based on the strength of the peak at 400 nm, the initial concentration (C_0) of 4-nitrophenolate ions was calculated. At a certain reaction time, 3 mL of the mixture was taken out for UV-vis adsorption monitoring, and the concentration (C) was calculated. The correlation of $\ln(C/C_0)$ *versus* the reduction time t was estimated to be linear, and the slope was estimated as the apparent reaction rate constant (k_{app}). k_{app} is the average values calculated from three runs of a certain measurement. Following the above steps, the flow rate of CO_2 was controlled at 10 mL min^{-1}, 15 mL min^{-1}, 20 mL min^{-1}, 25 mL min^{-1}, 30 mL min^{-1}, 40 mL min^{-1} and 50 mL min^{-1}, respectively, to carry out catalytic reaction. With the progress of the reaction, the color of the solution gradually fades from yellow to colorless. Noteworthy, after bubbling CO_2 for a minute, the pH of the mixture will be less than 6.7. At the same time, there was a peak at 317 nm, the peak of 4-nitrophenol, indicating that $NaBH_4$ was consumed by CO_2 and the catalytic reaction was not complete. Therefore, a certain amount of $NaBH_4$ should be added. At the end of the reaction, silver nanoparticles were separated by bubbling N_2.

Characterization

UNICO UV-4802 double-beam spectrophotometer (UV-vis spectroscopy) was used to observe the location and migration of silver nanoparticle peaks. The full width at half-maximum (FWHM) values of the UV-vis spectra were measured by previous methods.[57] In the catalytic reduction of 4-nitrophenol, UV-visible spectroscopy can be used to determine its reduction.

Infrared spectra were registered on a Nicolet MX-1E FTIR (USA) spectrophotometer in the scanning range of 4000–400 cm^{-1} using KBr pellet method.

The ^1H NMR of the polymer was measured using a Nuclear Magnetic Resonance Spectrometer (AV CORP300, Bruker, Germany). The polymer was purified according to its solubility in $CDCl_3$, and the molecular structure of the polymer was determined from the corresponding chemical shift and integral area in the ^1H NMR.

The molecular weight and the molecular weight distribution of the polymers were determined using a gel permeation chromatography (GPC) system equipped with a Waters 515 pump and a 2410 detector. The column temperature was set at 25 °C and the THF was used as the mobile phase. Polystyrene (PSt) was used as the reference material.

Thermal gravimetric analysis (TGA, 299-F1, NETZSCH, Germany) was used to test the polymer modified silver nanoparticles in the polymer content. The sample was heated to a temperature of 800 °C at a rate of 10 °C min^{-1} in a nitrogen atmosphere (flow rate 20 mL min^{-1}). The dialyzed dark brown concentrated mixture was purged with N_2 for 1 h and centrifuged at 10 000 rpm for 5 minutes, the upper layer was discarded, washed with deionized water and centrifuged. After three times, the mixture was suction filtered and the solid sample was vacuum dried at 50 °C for 24 hours prior to TGA and XRD characterizations.

The zeta potential values of silver colloid were measured with zetameter ZetaPALS (Brookhaven, USA). Each test was carried out for five times and the average values were taken as the final results.

X-ray diffraction (XRD) patterns of AgNPs hybrids was recorded using a RigakuDMAX2200 with Ni-filtered Cu K_α radiation over a scanning range of 30 to 80° at an X-ray power of 40 kV and 40 mA.

The conductivity of Ag–P1 dispersion was measured with a DDS-11A conductometer (Chengdu Fangzhou Instrument) at 25 °C, and the average values were calculated from three runs of a certain measurement.

Transmission electron microscope (Holland, Philips Company, Tecnai12) was used to observe the particle size distribution of silver nanoparticles. The size distributions of each sample were determined at least 1000 particles from photographs of the TEM images by image analysis software (Nano Measurer). As for negative staining TEM, the sample was stained with phosphotungstic acid for TEM observation.

Results and discussion

Synthesis and characterization

To bestow the CO_2-switchable property on AgNPs, CO_2-responsive polymer was needed. Based on previous reports, polymer with amidine[34,35] or tertiary amine groups[36–40] exhibits CO_2-responsive characteristic. However, as for amidine-based polymer, heating is usually needed to expel the captured CO_2.[34,35] In contrast, polymer containing tertiary amine groups could realize reversible switchability in the same condition upon alternate treatment of CO_2 and N_2.[36–40] PDEAEMA was a typical tertiary amine type CO_2-responsive polymer.[36,37] Thus PDEAEMA was synthesized through RAFT polymerization, as RAFT not only is a powerful and versatile controlled radical polymerization technique, enables precise control over the MW, MW distribution, but also introduce trithioester group to the end of polymer.[49,50] Detailed preparation and characterization procedures can be found in ESI.†

To form CO_2-switchable AgNPs, the silver nanoparticles were prepared by reducing silver nitrate ($AgNO_3$) with $NaBH_4$ in the presence of the PDEAEMA. Meanwhile, trithioester end group of PDEAEMA was reduced to thiol group with $NaBH_4$,[46–49] providing the necessary for chemical attaching PDEAEMA on the surface of AgNPs (Scheme 1). With such one-pot protocol, a series of AgNPs–PDEAEMA (Ag–P) dispersion were prepared by varying the molar ratios (1 : 6, 1 : 12 and 1 : 24) of PDEAEMA to $AgNO_3$, as shown in Table 1. For characterization and storage, AgNPs hybrids were transferred from methanol to aqueous environment by bubbling CO_2. And three dark brown dispersion were finally obtained (insert, Fig. 1), indicative of the formation of AgNPs.[51]

Table 1 Characterization of the Ag–NPs in the PDEAEMA solutions

Sample[a]	[PDEAEMA] : [$AgNO_3$][b]	% PDEAEMA/% Ag[c]	Average diameter of Ag–NPs[d], nm
Ag–P1	1 : 6	90/10	8.51 ± 2.8
Ag–P2	1 : 12	84/16	10.06 ± 3.7
Ag–P3	1 : 24	71/29	14.16 ± 6.6

[a] Ag–P refers to PDEAEMA polymer-stabilized silver nanoparticles. [b] Molar ratios of PDEAEMA to $AgNO_3$. [c] Weight percentage, determined by TGA. [d] Estimated from TEM images.

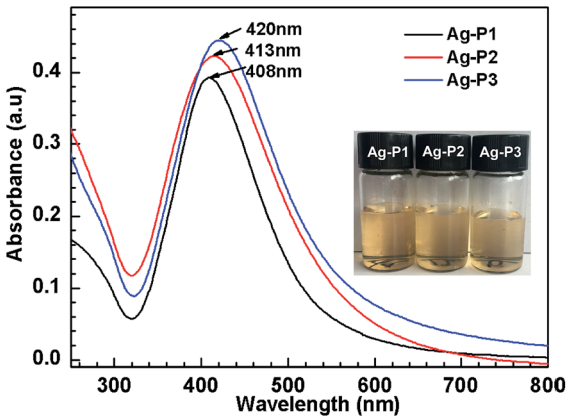

Fig. 1 UV-vis spectra of Ag–P1, Ag–P2 and Ag–P3 in water after bubbling CO_2 at 25 °C. The inset images of the hybrids solution refer to corresponding samples. The concentration of hybrids is 0.06 mg mL^{-1}.

To characterize the formation of AgNPs hybrids, UV-vis spectroscopy which is known for the sensitivity to the size, size distribution and morphology of metal nanoparticles[51,52] was employed. As shown in Fig. 1, single absorption peak is found in the region of 320–600 nm, resulting from intense surface plasmon resonances (SPR) of the obtained AgNPs.[53] It is noteworthy that the λ_{max} gradually increases with increasing the silver contents of Ag-polymer dispersion. Usually, λ_{max} of AgNPs are biased to shift to longer wavelengths with increasing nanoparticle size,[52] suggesting that the AgNPs size increases slightly upon increasing the silver contents. This may arise from the increased collision frequency due to the formation of more Ag atoms.[46,54] Furthermore, the full width at half-maximum (FWHM) could be calculated from the UV-vis spectra, since FWHM is useful to evaluate the polydispersity of AgNPs.[46,56] The FWHM value of Ag–P1 is 105 nm, which are similar to or slightly smaller than those previously reported for AgNPs.[46,52,55] Correlating with symmetric absorption peaks, this implies that the size of Ag–P1 is uniform.[56] Compared with Ag–P1, the FWHM for Ag–P2 (118 nm), Ag–P3 (124 nm) become wider, suggesting that the polydispersity of the hybrids increased with increasing the silver ratio.

In order to get more direct information on the size, size distribution and morphology of AgNPs, TEM observations were performed. Fig. 2 shows TEM images and size distribution histograms of three AgNPs. One can find that the AgNPs hybrids display good dispersion and a spherical shape. With total 1000 particles counted by an image analysis software (Nano Measure) on number distribution, we found Ag–P1 have an average size of 8.51 ± 2.8 nm with a narrow distribution. With increasing the silver ratio, the size and size distribution become bigger. The sizes of the other two AgNPs are 10.06 ± 3.7 nm and 14.16 ± 6.6 nm, respectively. The TEM results are in good agreement with those of the UV-vis spectra analysis. Thus the size and size distribution of as obtained AgNPs can be easily modulated by varying the molar ratio of polymers to $AgNO_3$. In addition, XRD was carried out to confirm the structure of AgNPs. As illustrated in Fig. S3,† their XRD pattern of AgNPs shows characteristic diffraction peaks for metallic silver [111], [200], [220] and [311] facets, indicative of the formation of pure Ag.[46,55,57,58]

As stated above, the AgNPs were clearly observed by TEM. However, the grafted PDEAEMA were not observed under TEM

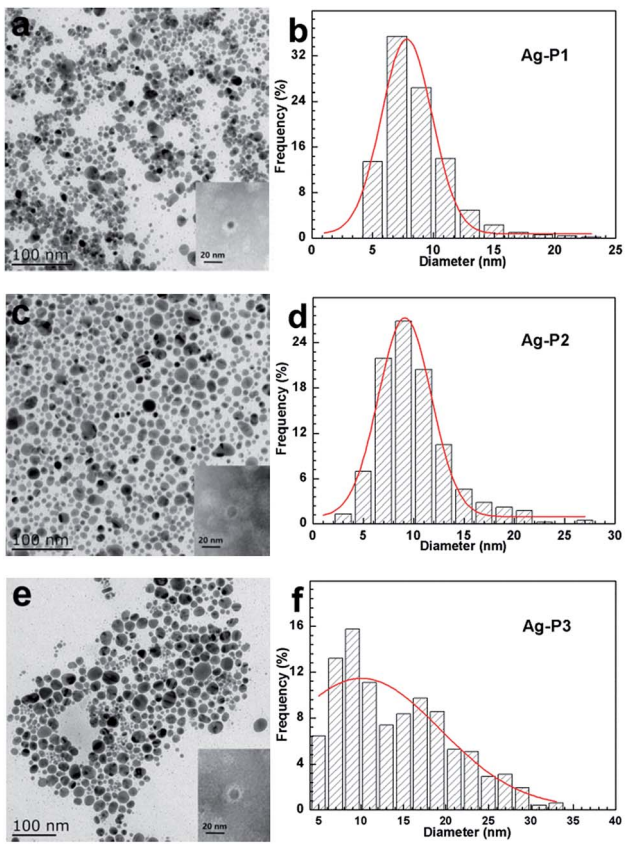

Fig. 2 TEM images of Ag–P1 (a), Ag–P2 (c) and Ag–P3 (e) in water and particle size distribution histograms of silver particles evaluated from the corresponding TEM images (b, d and f). The inset TEM images of the sample negatively staining with phosphotungstic acid.

observation, which may attribute to the polymer with lower atomic mass.[55] To confirm that PDEAEMA was grafted onto the surface of AgNPs, FT-IR spectroscopy was employed. As given in Fig. S4,† The IR spectra of the nanoparticles and the PDEAEMA are similar to one another, indicating that the polymer molecules have indeed grafted onto AgNPs. However, a remarkable difference in the peak intensity is found between the peaks in polymer and the hybrids. Those peaks correspond to the stretching mode of C=S (1062 cm^{-1}) and $-CH_2-S-$ (725 cm^{-1}).[49] After reaction, C=S was disappeared because the trithioester group was reduced to thio group. The decreased intensity for $-CH_2-S-$ is believed to be that the thiol end group of the polymer on the nanoparticle form a relatively close packed thiol layer and molecular motion is constrained,[56] which suggesting that polymer attached to AgNPs surface through a chemical bond between S ions and Ag atoms.

To determine the relative amount of PDEAEMA on AgNPs, thermal gravimetric analysis (TGA) measurement was carried out. From the TGA curve given in Fig. 3, the weight percentage of PDEAEMA in the Ag–P1, Ag–P2, Ag–P3 hybrids were *ca.* 90 wt%, 84 wt%, 71 wt%, respectively, from which we could calculate that one AgNPs was wrapped by roughly 2000 polymer chains (see ESI†). To visualize the polymer on nanoparticles, AgNPs samples treated with negative staining technique was used for TEM observation, which provides reverse-contrast negative electron optical images for the unstained component.[55] One can find that black AgNPs dot surrounded by the brighter polymer part, showing typical cocoon-like morphology (inset, Fig. 2). The thickness of observed PDEAEMA layer is about 6–10 nm, indicating that the polymers were attached to AgNPs. Compared with Ag–P2 and Ag–P3, Ag–P1 has smaller size and narrower size distribution. Therefore, in the following experiments, we will mainly focus on Ag–P1.

In addition, the stability of AgNPs in aqueous environment is important for their application.[55,56] To detect the stability of the PDEAEMA-protected AgNPs in water, we measured the absorption spectra of one of the AgNPs hybrids systems (Ag–P1) with the same concentration at different times. As shown from Fig. S5,† there is no obvious difference in the shape, position, and symmetry of the absorption peak during 12 months, indicative of the long-term stability of the hybrid.

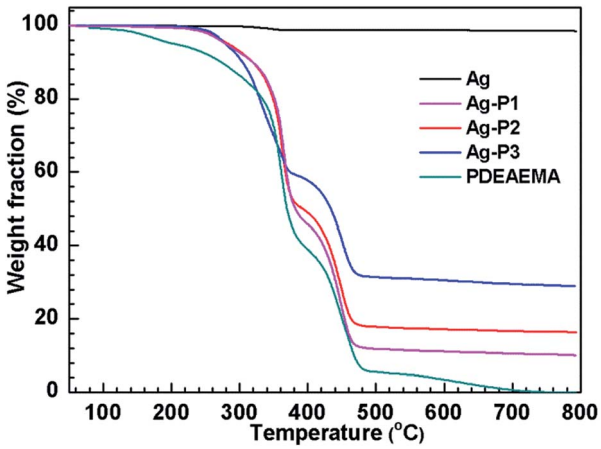

Fig. 3 TGA for Ag, Ag–P1, Ag–P2, Ag–P3 and PDEAEMA.

CO_2-switchable behavior of AgNPs hybrids

Hydrophobic–hydrophilic transition in immiscible mixed solvents. We found previously that the PDEAEMA itself can undergo a hydrophobic–hydrophilic transition by the stimulation of CO_2,[39] and now it is natural to examine whether the AgNPs coated with PDEAEMA has analogous transition. Fig. 4 compares the appearance of Ag–P1 in the mixed solvent of water/dichloromethane (DCM) (1 : 1, v/v) in the presence and in the absence of CO_2, respectively. In the former case, the dispersion separates into two phases; the upper layer is brown while the lower one is transparent, indicating that Ag–P1 reside in the top water layer (inset, Fig. 4a). However, when N_2 is bubbled into the mixing solution to expel CO_2, the upper water phase turns into transparent, suggesting that the AgNPs hybrids move from the aqueous phase to the organic one, *i.e.*, the Ag–P1 hybrids transform from hydrophilic to hydrophobic, and thus dissolve in the organic layer (inset, Fig. 4b).

During this process, UV-vis spectroscopy was used to investigate the dispersion state in the mixed solvent. As the hybrids was treated with CO_2, the upper aqueous solution exhibited SPR at 408 nm (Fig. 4a), indicating that Ag–P1 hybrids were dispersed in the water phase. In contrast, the lower DCM solution shows no obvious signals in the range of 250–800 nm, suggesting no Ag–P1 presented in lower organic layer. When N_2 was bubbled into the biphasic solution, the UV-vis spectra of the

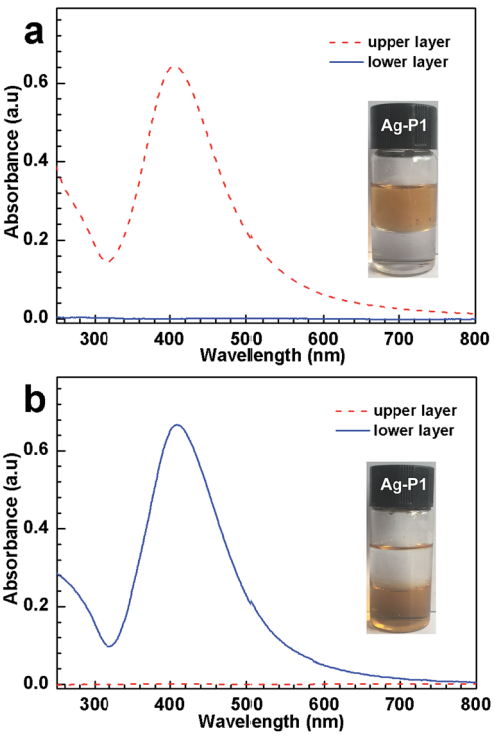

Fig. 4 Hydrophobic–hydrophilic transition of Ag–P1 hybrids (0.08 mg mL^{-1}, 25 °C) in DCM/water (1 : 1, v/v) monitored by the UV-vis spectrum: (a) treated with CO_2 and (b) bubbling N_2.

two phases was reversed, that is, the lower DCM phase exhibits strong SPR peak (Fig. 4b), while no signals appeared in the upper aqueous solution. These UV-vis spectra clearly show that Ag–P1 experiences a hydrophobic–hydrophilic transition. Based on these macroscopic results, it is noteworthy that Ag–P1 can switch between aqueous media and organic solvents, which is convenient for separation/collection.

Switchable dispersibility in water. Having established that AgNPs hybrids were dispersed in aqueous environment, we wonder if the dispersibility of AgNPs hybrids could be reversibly controlled by the stimulation of CO_2. Thus, we extend the response of AgNPs hybrids to CO_2 in pure water. As stated above, AgNPs hybrids can dissolved in aqueous environment under the treatment of CO_2. Nevertheless, after bubbling N_2 for 60 min at room temperature, the hybrids precipitated from aqueous solution (inset, Fig. 6a); when CO_2 was bubbled for 10 min again, the hybrid aqueous solution became homogeneous accordingly. Such a procedure is still effective beyond three cycles of bubbling N_2 and CO_2, suggesting that the dispersion/aggregation state of hybrids can be switchablely controlled.

To further reveal the dispersion state of the hybrids, UV-vis spectroscopy, was employed to monitor the variation of absorbance of hybrid suspension after bubbling and removing CO_2, respectively. As shown in Fig. 5a, a strong SPR absorbance was observed after bubbling CO_2. With bubbling N_2, on the other hand, the absorbance gradually decreased, and concomitantly the SPR peak showed blue shift (from 408 nm to 425 nm), indicative of aggregation and precipitation.[52,56] In addition, the FWHM values of the spectra increase with time of bubbling N_2 (Fig. 5c), implying the formation of AgNPs aggregates with larger size and broad size distribution. In order to get more direct information on the aggregation state of AgNPs hybrids in water, TEM were performed. An obvious aggregation state of the AgNPs hybrids can be observed (Fig. S6†), which is in good agreement with the abovementioned results. When the dispersion was treated with CO_2 again, the SPR peak and its FWHM reinstated (Fig. 5b and c), indicating that AgNPs hybrids were re-dispersed again.

To elucidate the dispersed/aggregated transition, electrical conductivity measurements were performed to monitor the change of conductivity for the suspension when cyclically bubbling CO_2 and N_2 (Fig. 6a). When CO_2 was introduced into dispersion, the conductivity sharply rises from about *ca.* 5.8 to ~130 μS cm^{-1}, with a net enhancement of about 124 μS cm^{-1}, which must be due to the tertiary amine groups in PDEAEMA reacting with CO_2 in water to form charged ammonium bicarbonate.[37–42] When CO_2 was displaced by N_2, the conductivity recovered to its original value, and this reversible change in conductivity could be repeated several times, which amply demonstrate that the response of the suspension to CO_2 was fully reversible and reproducible.[34]

To further confirm that ionization happened on the cocoon of the hybrids, zeta potential of the silver colloidal solution has been measured. The zeta potential for the particle treated with CO_2 reached +60.2 mV, as exhibited in Fig. 6b, supporting the formation of positive ammonium ions of the surface coated polymers. After removing CO_2 by purging N_2, the zeta potential decreases with increasing in the time of purging N_2, and finally reduced to +0.66 mV (Fig. 6b), suggesting that positive ammonium ions of the polymer cocoon were mostly deprotonated due to the deportation of the CO_2.

Responsive mechanism. On the basis of the above results, it is reasonable to speculate that AgNPs were dispersed in solution by adsorbed PDEAEMA owing to the chemical bond formed

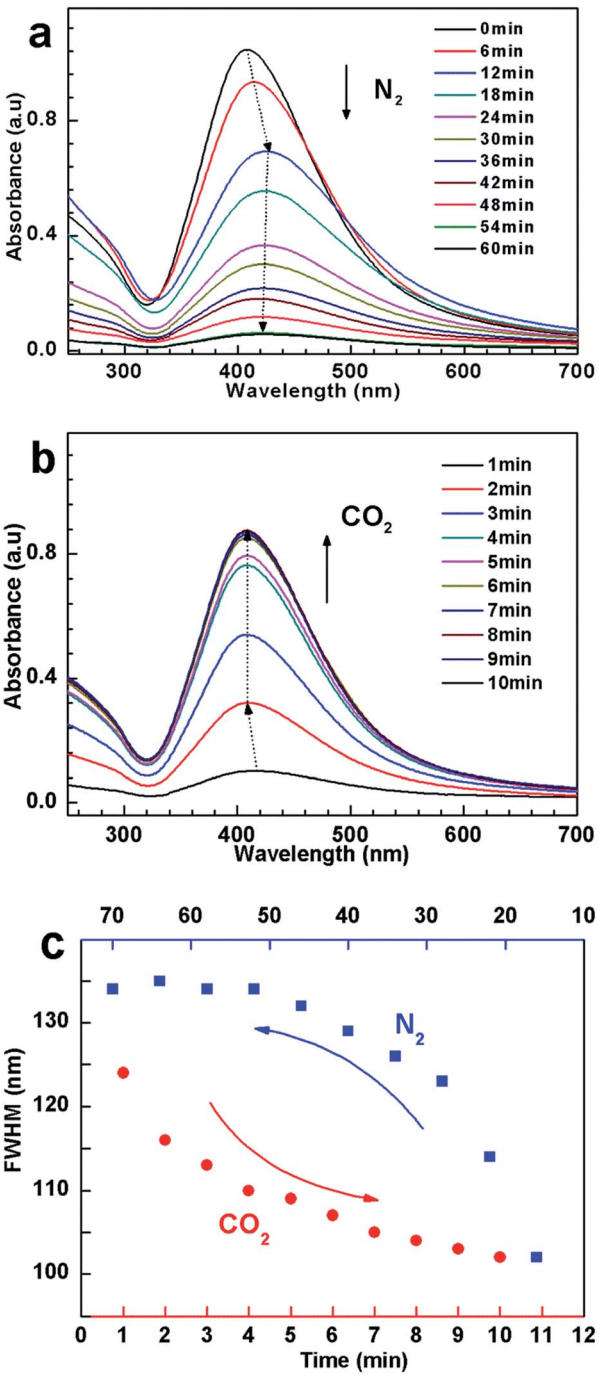

Fig. 5 UV-vis spectra changes of 0.1 mg mL^{-1} Ag–P1 aqueous dispersion with (a) N_2 bubbling (120 mL min^{-1}) and (b) CO_2 bubbling (100 mL min^{-1}). (c) The cyclic changes of FWHM values with N_2 and CO_2 bubbling, which was calculated from UV-vis spectra.

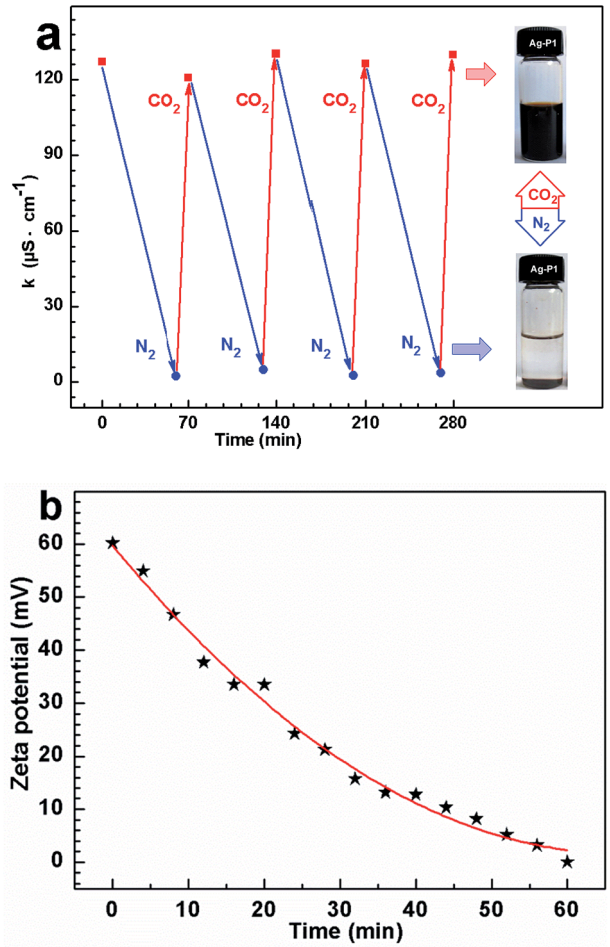

Fig. 6 (a) Cyclic changes in conductivity of Ag–P1 aqueous dispersion measured at 25 °C with treatment of CO_2 and N_2, where the concentrations of Ag–P1 is 2.23 mg mL^{-1}. (b) The zeta potential of Ag–P1 aqueous dispersion at different time after bubbling N_2 at 25 °C.

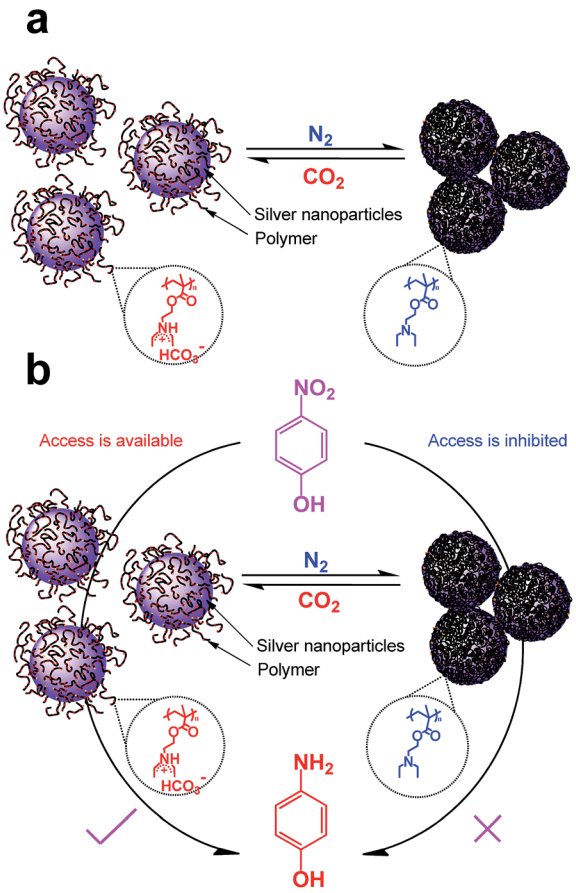

Scheme 2 Schematic illustration of the AgNPs hybrids response to the stimulus of CO_2 (a), and switch and tune the catalytic activity for reduction of 4-nitrophenol (b).

between S ions and Ag atoms, as shown in Scheme 1. The CO_2-switchable dispersion of AgNPs hybrids in mixed solvent is ascribed to the polymer cocoon with hydrophobic backbone and CO_2-responsive tertiary amine groups. As illustrated in Scheme 2a, when treated with CO_2, the tertiary amine groups along PDEAEMA convert into charged ammonium bicarbonates,[37–42] making PDEAEMA hydrophilic and thus leading the hybrids to disperse in aqueous media. Otherwise, after removing CO_2, the PDEAEMA become neutral and hydrophobic; therefore DCM is a good solvent and the hybrids shift from water to DCM.

The reversible dispersion/aggregation states of AgNPs hybrids controlled by CO_2 in water could also be understood based on the CO_2-responsive behaviour of PDEAEMA. As shown in Scheme 2a, the tertiary amine groups of PDEAEMA coated on AgNPs were protonated when reacted with CO_2 in water, leading an extended conformation of the polymer. Thus the interchain electrostatic repulsion and the steric hindrance among the AgNPs protected by the charged PDEAEMA should allow the long-term dispersing in water. After the removal of CO_2, the electrostatic repulsion of PDEAEMA disappears owing to an opposite deprotonation effect,[36,37] thus diminishing the polymer–polymer electrostatic repulsions and increasing the interaction among polymer chains,[34] resulting in larger particles, and precipitate from aqueous solution.

Application in catalysis

As the AgNPs hybrids exhibit sensitive to CO_2-switchable behaviour, it is interesting to see if the hybrids can be used as a gas-tunable catalysis. Here, in order to evaluate the catalytic activity of the as-obtained AgNPs hybrids, the reduction of 4-nitrophenol, to 4-aminophenol by $NaBH_4$ was used as model reaction. Because 4-nitrophenol is one of the most refractory pollutants in industrial wastewaters while 4-aminophenol is a commercially important intermediate for the manufacture of analgesic and antipyretic drugs.[59] In addition, the reactant 4-nitrophenol could transfer into 4-nitrophenolate ion at high pH and shows characteristic peak at 400 nm; and the product 4-aminophenol gives a typical absorption at 300 nm, which is easily monitored by UV-vis measurement.[9,55,59]

Fig. S7a† shows the time-dependent UV spectra for the reduction of 4-nitrophenol in presence of CO_2-treated AgNPs hybrids. One can find that the peak height at 400 nm exhibit a slight decreases within 40 min (Fig. S7a†), indicating a very

low conversion of 4-nitrophenol. Based on the absorption at 400 nm values, linear correlation between $\ln(C/C_0)$ (C is the concentration at a certain reaction time and C_0 is the initial concentration of 4-nitrophenolate ions) *versus* reaction time was obtained (Fig. S7a†), indicating that such a catalytic reduction follows a pseudo-first-order law. The apparent reaction rate constant (k_{app}) was calculated from linear and is only 1.15×10^{-5} s^{-1}. This result confronts earlier observations that CO_2-bubbled AuNPs protected with PDEAEMA still exhibits a high catalytic activity for 4-nitrophenol.[41,42] This may arise from that the density of PDEAEMA grafted on AgNPs hybrids, *ca.* 2000 polymer chains in one particle as aforedescribed, is higher than that of reported ones, though the previous papers did not provide this data.[41,42] When CO_2-treated AgNPs hybrids was introduce into the solution, the charged ammonium bicarbonates would be deprotonated because the basic $NaBH_4$ reacted with carbonic acid formed by CO_2 and water (*i.e.*, $NaBH_4 + H^+ + 3H_2O = Na^+ + 4H_2\uparrow + H_3BO_3$). Thus PDEAEMA cocoon became hydrophobic and wrapped AgNPs tightly, which inhibited access to the catalytic sites of AgNPs (Scheme 2b).

To open the access for 4-nitrophenol, we tried to bubble CO_2 into the mixing solution. Firstly, we wonder whether 4-nitrophenol could be reduced by CO_2. CO_2 was bubbled into the mixing solution of 4-nitrophenol and $NaBH_4$ (without AgNPs hybrids). After bubbling CO_2 for 50 min, the peak height at 400 nm has no change (Fig. S8, ESI†), suggesting that 4-nitrophenol could not be reduced by CO_2 in absent of AgNPs hybrids. In contrast, CO_2 was purged into the mixture in presence of Ag–P1 hybrids. When the flow rate of CO_2 is 10 mL min^{-1}, it was found that the absorption at 400 nm decreased slowly within the first 18 min, and then dropped fast to nearly zero (Fig. S7b†). Meanwhile, the peak of 4-aminophenol at 300 nm was observed,[42,55] implying that 4-nitrophenol was reduced to 4-aminophenol. It clearly shows an induction time before the conversion of reactants into products takes place (Fig. 7a and S7b†). After deducting the induction time (t_i), the k_{app} is 1.57×10^{-3} s^{-1} and bigger than that of without bubbling CO_2. This result suggests that access to the encapsulated AgNPs was opened, since polymer chains contacted with CO_2 and extended in solution. When the flow rate increased, the induction time decreased and disappeared at 25 mL min^{-1} (Fig. 7a). And concomitantly the k_{app} increased with the flow rate, and reach to *ca.* 3.6×10^{-3} s^{-1} at 50 mL min^{-1} (Fig. S7h†), which is close to gold nanoparticle reaction rate constant.[42] The k_{app} as function of CO_2 flow rate was presented in Fig. 7b. Two linear regimes in the k_{app} curve are found: a monotonous linear increase in k_{app} is evidenced while CO_2 flow within 30 mL min^{-1}, after which it is slight change.

To elucidate this variation, pH value of the solution under bubbling CO_2 was tested, since the degree of protonation increases with decreasing of pH.[37] As exhibited in Fig. S9,† the pH decreased with bubbling CO_2 and maintained at *ca.* 7 for catalysis. Note that if the pH was less than 6.7, the peak at 317 nm ascribed to 4-nitrophenol would appear, which would affect the catalytic reaction.[60] During the reaction, additional $NaBH_4$ should be added to compensate that of consumed by

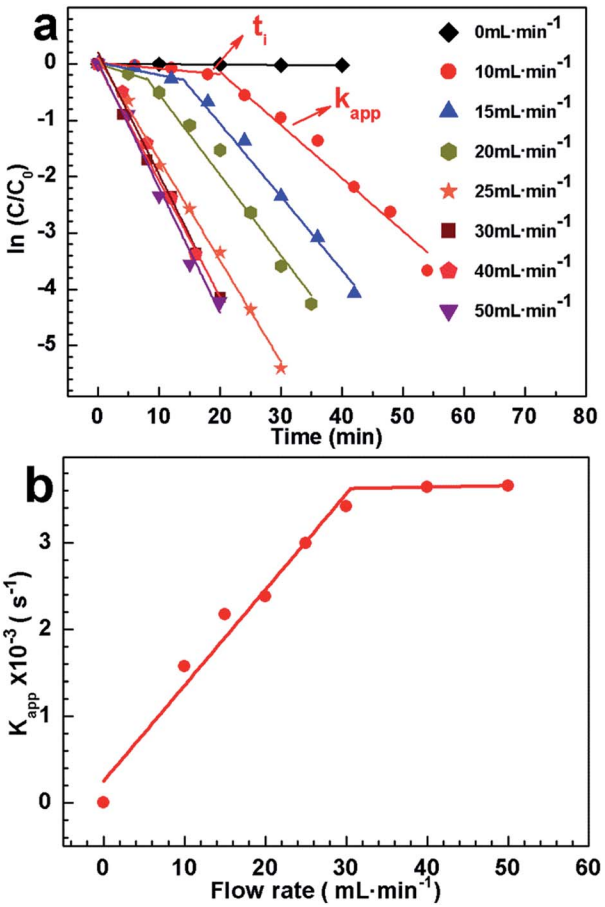

Fig. 7 (a) The plots of $\ln(C/C_0)$ *versus* the time t at different flow rate of CO_2 stimuli. (b) The variation of the apparent reaction rate constant (k_{app}) at different CO_2 flow rate. The concentrations of 4-NP and Ag–P1 are 0.0139 mg mL^{-1} and 2×10^{-3} mg mL^{-1}, respectively.

CO_2 and keep pH stable. Besides, it clearly shows that the time for decreasing pH to *ca.* 7 increases with low flow rate, which may cause the induction time. As there was no obvious difference on pH for catalysis at different flow rate, the hybrid should show a similar protonation and has similar k_{app}. A possible explanation for increasing k_{app} is that the frequency for PDEAEMA cocoon contacting with CO_2 increased under the high CO_2 flow rate, which is favourable to opening the access to AgNPs. Such preliminary findings, particularly the linearity found in the flow rate below 30 mL min^{-1}, imply that the catalytic activity of Ag–P1 hybrids can be switched and monotonously tuned by varying the flow rate of CO_2 purged into the reaction system.

Conclusions

In summary, we have prepared CO_2-switchable AgNPs hybrids by one-pot reducing $AgNO_3$ and trithioester terminated PDEAEMA with $NaBH_4$. Apart from the long-term stability, the size and size distribution of AgNPs hybrids can be easily modulated by varying the molar ratio of polymers to $AgNO_3$. The

hybrids not only exhibit hydrophobic–hydrophilic transitions in immiscible mixed solvents, but also undergo a switchable dispersion/aggregation states upon alternate treated with CO_2 and N_2. In addition, we have demonstrated that the catalytic activity of the hybrids for the reduction of 4-nitrophenol can be switched and monotonously tuned by varying the flow rate of CO_2 purged into the reaction system, which may open a new avenue for tailoring the catalytic activity of metal nanoparticles toward a given reaction. The strategies described in this work can also be used to functionalize other nanoparticles in a quick and easy way.

Conflicts of interest

There are no conflicts to declare.

Acknowledgements

This project is supported by Open Fund (PLN1508) of State Key Laboratory of Oil and Gas Reservoir Geology and Exploitation (Southwest Petroleum University) and National Natural Science Foundation of China (51563009, 21465011, 21464006, 21464005). W. M. thanks the financial support from the Innovation Fund Designated for Graduate Students of Jiangxi Province (YC2016-S265).

Notes and references

1 P. Christopher, H. Xin and S. Linic, *Nat. Chem.*, 2011, **3**, 467–472.
2 H. Song, *Acc. Chem. Res.*, 2015, **48**, 491–499.
3 A. Corma and H. Garcia, *Chem. Soc. Rev.*, 2008, **37**, 2096–2126.
4 Y. Xu, L. Chen, X. Wang, W. Yao and Q. Zhang, *Nanoscale*, 2015, **7**, 10559–10583.
5 J. Zhou, J. Ralston, R. Sedev and D. A. Beattie, *J. Colloid Interface Sci.*, 2009, **331**, 251–262.
6 A. Shahzad, W.-S. Kim and T. Yu, *RSC Adv.*, 2015, **5**, 28652–28661.
7 L. Xie, M. Chen and L. Wu, *J. Polym. Sci., Part A: Polym. Chem.*, 2009, **47**, 4919–4926.
8 J.-T. Zhang, G. Wei, T. F. Keller, H. Gallagher, C. Stötzel, F. A. Müller, M. Gottschaldt, U. S. Schubert and K. D. Jandt, *Macromol. Mater. Eng.*, 2010, **295**, 1049–1057.
9 S. Li, D. Lin, J. Zhou and L. Zha, *J. Phys. Chem. C*, 2016, **7**, 343–349.
10 K. J. Rao and S. Paria, *ACS Sustainable Chem. Eng.*, 2015, **3**, 483–491.
11 K. Layek, M. L. Kantam, M. Shirai, D. Nishio-Hamane, T. Sasaki and H. Maheswaran, *Green Chem.*, 2012, **14**, 3164–3174.
12 S. Wunder, F. Polzer, Y. Lu, Y. Mei and M. Ballauff, *J. Phys. Chem. C*, 2010, **114**, 8814–8820.
13 T. Yao, T. Cui, H. Wang, L. Xu, F. Cui and J. Wu, *Nanoscale*, 2014, **6**, 7666–7674.
14 R. Rajesh, S. S. Kumar and R. Venkatesan, *New J. Chem.*, 2014, **38**, 1551–1558.
15 E. Kumacheva, *Nat. Mater.*, 2012, **11**, 665–666.
16 S. Cao, J. Chen, Y. Ge, L. Fang, Y. Zhang and A. P. Turner, *Chem. Commun.*, 2014, **50**, 118–120.
17 G. Marcelo, M. Lópezgonzález, F. Mendicuti, M. P. Tarazona and M. Valiente, *Macromolecules*, 2014, **47**, 6028–6036.
18 J. Zhang, M. Zhang, K. Tang, F. Verpoort and T. Sun, *Small*, 2013, **10**, 32–46.
19 A. Döring, W. Birnbaum and D. Kuckling, *Chem. Soc. Rev.*, 2013, **42**, 7391–7420.
20 Y. Zhou, M. Zhu and S. Li, *J. Mater. Chem. A*, 2014, **2**, 6834–6839.
21 D. A. Burnat, R. Kontic, L. Holzer, P. Steiger, D. Ferri and A. Heel, *J. Mater. Chem. A*, 2016, **4**, 11939–11948.
22 Z. Liu, X. Tong, J. Liu and S. Xue, *Catal. Sci. Technol.*, 2016, **6**, 1214–1221.
23 R. Begum, K. Naseem and Z. H. Farooqi, *J. Sol-Gel Sci. Technol.*, 2016, **77**, 497–515.
24 X. Jiang, D. A. Xiong, Y. An, P. Zheng, W. Zhang and L. Shi, *J. Polym. Sci., Part A: Polym. Chem.*, 2010, **45**, 2812–2819.
25 J. Bigot, B. Charleux, G. Cooke, D. Fournier and P. Woisel, *J. Am. Chem. Soc.*, 2010, **132**, 10796–10801.
26 R. K. O'Reilly, C. J. Hawker and K. L. Wooley, *Chem. Soc. Rev.*, 2006, **35**, 1068–1083.
27 J. Zhang, S. Xu and E. Kumacheva, *Adv. Mater.*, 2005, **17**, 2336–2340.
28 Z. Chen, Z. M. Cui, C. Y. Cao, W. D. He, L. Jiang and W. G. Song, *Langmuir*, 2012, **28**, 13452–13458.
29 S. Li, G. Yi and A. P. F. Turner, *Adv. Funct. Mater.*, 2011, **21**, 1194–1200.
30 M. Z. And and W. Zhang, *J. Phys. Chem. C*, 2008, **112**, 6245–6252.
31 Z. Chen, L. Xu, Y. Liang and M. Zhao, *Adv. Mater.*, 2010, **22**, 1488–1492.
32 C. Xiao, S. Chen, L. Zhang, S. Zhou and W. Wu, *Chem. Commun.*, 2012, **48**, 11751–11753.
33 X. Chen, Y. An, D. Zhao, Z. He, Y. Zhang, J. Cheng and L. Shi, *Langmuir*, 2008, **24**, 8198–8204.
34 Z. Guo, Y. Feng, S. He, M. Qu, H. Chen, H. Liu, Y. Wu and Y. Wang, *Adv. Mater.*, 2013, **25**, 584–590.
35 Z. Guo, Y. Feng, Y. Wang, J. Wang, Y. Wu and Y. Zhang, *Chem. Commun.*, 2011, **47**, 9348–9350.
36 Q. Yan, J. Wang, Y. Yin and J. Yuan, *Angew. Chem., Int. Ed. Engl.*, 2013, **52**, 5070–5073.
37 D. Han, X. Tong, O. Boissière and Y. Zhao, *ACS Macro Lett.*, 2013, **1**, 57–61.
38 P. G. Jessop, S. M. Mercer and D. J. Heldebrant, *Energy Environ. Sci.*, 2012, **5**, 7240–7253.
39 H. Liu, Z. Guo, S. He, H. Yin, C. Fei and Y. Feng, *Polym. Chem.*, 2014, **5**, 4756–4763.
40 M. Ying, K. Promthaveepong and L. Nan, *Anal. Chem.*, 2016, **88**, 8289–8293.
41 J. Zhang, D. Han, H. Zhang, M. Chaker, Y. Zhao and D. Ma, *Chem. Commun.*, 2012, **48**, 11510–11512.
42 A. Feng, Y. Wang, L. Peng, X. Wang and J. Yuan, *RSC Adv.*, 2016, **6**, 97030–97035.

43 H. Song, R. M. Rioux, J. D. Hoefelmeyer, R. Komor, K. Niesz, M. Grass, P. Yang and G. A. Somorjai, *J. Am. Chem. Soc.*, 2006, **128**, 3027–3037.
44 G. J. Leong, A. Ebnonnasir, M. C. Schulze, M. B. Strand, C. Ngo, D. Maloney, S. L. Frisco, H. N. Dinh, B. Pivovar and G. H. Gilmer, *Nanoscale*, 2014, **6**, 11364–11371.
45 E. Shahbazali, V. Hessel, T. Noël and Q. Wang, *Nanotechnol. Rev.*, 2014, **3**, 65–86.
46 Y. Wu, S. He, Z. Guo and Y. Feng, *Polym. Sci.*, 2013, **55**, 634–642.
47 Y. Sun, Y. Liu, G. Zhao, X. Zhou, J. Gao and Q. Zhang, *J. Mater. Sci.*, 2008, **43**, 4625–4630.
48 J. Raula, J. Shan, M. Nuopponen, A. Niskanen, H. Jiang, E. I. Kauppinen and H. Tenhu, *Langmuir*, 2003, **19**, 3499–3504.
49 J. T. Lai, D. Filla and R. Shea, *Macromolecules*, 2002, **35**, 6754–6756.
50 G. Moad, E. Rizzardo and S. H. Thang, *Aust. J. Chem.*, 2012, **65**, 985–1076.
51 S. Pal, Y. K. Tak and J. M. Song, *Appl. Environ. Microbiol.*, 2007, **73**, 1712–1720.
52 R. Brause, H. Möltgen and K. Kleinermanns, *Appl. Phys. B*, 2002, **75**, 711–716.
53 J. A. Creighton and D. G. Eadon, *J. Chem. Soc., Faraday Trans.*, 1991, **87**, 3881–3891.
54 D.-H. Chen and Y.-W. Huang, *J. Colloid Interface Sci.*, 2002, **255**, 299–302.
55 S. He, H. Chen, Z. Guo, B. Wang, C. Tang and Y. Feng, *Colloids Surf., A*, 2013, **429**, 98–105.
56 S. He, J. Yao, P. Jiang, D. Shi, H. Zhang, S. Xie, A. S. Pang and H. Gao, *Langmuir*, 2001, **17**, 1571–1575.
57 J. Yang, H. Yin, J. Jia and Y. Wei, *Langmuir*, 2011, **27**, 5047–5053.
58 R. Shankar, L. Groven, A. Amert, K. W. Whites and J. J. Kellar, *J. Mater. Chem.*, 2011, **21**, 10871–10877.
59 Y. Lu, Y. Mei, M. Ballauff and M. Drechsler, *J. Phys. Chem. B*, 2006, **110**, 3930–3937.
60 L. A. Shah, A. Haleem, M. Sayed and M. Siddiq, *J. Environ. Chem. Eng.*, 2016, **4**, 3492–3497.